Journal of Virological Methods 265 (2019) 77–83

Contents lists available at ScienceDirect

Journal of Virological Methods

journal homepage: www.elsevier.com/locate/jviromet

A high-throughput inhibition assay to study MERS-CoV antibody interactions using image cytometry

Osnat Rosen[a,1], Leo Li-Ying Chan[b], Olubukola M. Abiona[a], Portia Gough[b], Lingshu Wang[a], Wei Shi[a], Yi Zhang[a], Nianshuang Wang[c], Wing-Pui Kong[a], Jason S. McLellan[c], Barney S. Graham[a,*], Kizzmekia S. Corbett[a,*]

[a] Vaccine Research Center, National Institute of Allergy and Infectious Diseases, National Institutes of Health, Bethesda, MD 20892, United States
[b] Department of Technology R&D, Nexcelom Bioscience LLC, Lawrence, MA 01843, United States
[c] Molecular Biosciences Department, University of Texas at Austin, Austin, TX 03755, United States

ARTICLE INFO

Keywords:
MERS-CoV
Antibody binding
Inhibition assay
Antibody neutralization
Image cytometry
Celigo

ABSTRACT

The emergence of new pathogens, such as Middle East respiratory syndrome coronavirus (MERS-CoV), poses serious challenges to global public health and highlights the urgent need for methods to rapidly identify and characterize potential therapeutic or prevention options, such as neutralizing antibodies. Spike (S) proteins are present on the surface of MERS-CoV virions and mediate viral entry. S is the primary target for MERS-CoV vaccine and antibody development, and it has become increasingly important to understand MERS-CoV antibody binding specificity and function. Commonly used serological methods like ELISA, biolayer interferometry, and flow cytometry are informative, but limited. Here, we demonstrate a high-throughput protein binding inhibition assay using image cytometry. The image cytometry-based high-throughput screening method was developed by selecting a cell type with high DPP4 expression and defining optimal seeding density and protein binding conditions. The ability of monoclonal antibodies to inhibit MERS-CoV S binding was then tested. Binding inhibition results were comparable with those described in previous literature for MERS-CoV spike monomer and showed similar patterns as neutralization results. The coefficient of variation (CV) of our cell-based assay was < 10%. The proposed image cytometry method provides an efficient approach for characterizing potential therapeutic antibodies for combating MERS-CoV that compares favorably with current methods. The ability to rapidly determine direct antibody binding to host cells in a high-throughput manner can be applied to study other pathogen-antibody interactions and thus can impact future research on viral pathogens.

1. Introduction

Coronaviruses (CoVs) thrive in animal reservoirs and represent a constant threat to human health. Six CoVs are currently known to infect humans; four of which, HKU1-CoV, 229E-CoV, NL63-CoV, and OC43-CoV, circulate endemically causing relatively mild respiratory disease that is rarely lethal (Corman et al., 2018). Zoonotic transmission of CoVs is associated with high mortality, exemplified by the 2012 emergence of Middle East respiratory syndrome coronavirus (MERS-CoV). Globally, MERS-CoV has resulted in 2249 laboratory-confirmed cases of infection, 798 of which have been fatal, and those statistics increase as the virus continues to cause outbreaks in the Middle East (WHO, 2018). Frequent regional outbreaks and pandemic potential of MERS-CoV support the need for prophylactic and therapeutic interventions. Monoclonal antibodies with broad neutralization activity could be used for both purposes.

MERS-CoV virions display surface spike (S) proteins. The two components of each S protomer include a head region (S1), which facilitates viral attachment, and a stem region (S2), which contains fusion machinery. MERS-CoV S1 is further compartmentalized into the receptor-binding domain (RBD), which binds to the host cell receptor dipeptidyl peptidase-4 (DPP4) and the N-terminal domain (NTD) (Du et al., 2013; Raj et al., 2013; Wang et al., 2013). Since RBD is involved in receptor binding, many antibody approaches thus far have focused on the MERS-CoV RBD subunit (Corti et al., 2015; Johnson et al., 2016; Niu et al., 2018; Wang et al., 2018, 2015; Wang et al., 2016; Yu et al., 2015). However, previous publications have also described neutralizing NTD- and S2-specific monoclonal antibodies (mAbs) (Chen et al., 2017;

* Corresponding authors.
E-mail addresses: bgraham@nih.gov (B.S. Graham), kizzmekia.corbett@nih.gov (K.S. Corbett).
[1] Current address: Department of Biotechnology, Israel Institute for Biological Research, Ness-ziona, Israel.

https://doi.org/10.1016/j.jviromet.2018.11.009
Received 20 June 2018; Received in revised form 16 November 2018; Accepted 19 November 2018
Available online 20 November 2018
0166-0934/ Published by Elsevier B.V.

Corti et al., 2015; Wang et al., 2018, 2015; Wang et al., 2016). With the recent structural elucidation of full-length MERS-CoV S trimer (Pallesen et al., 2017; Yuan et al., 2017), additional antibody targets have become more feasible, including other regions in S1 subunit, quaternary epitopes, and the exposed heptad repeat regions in S2 subunit. While many monoclonal IgGs show promise in animal challenge models (Chen et al., 2017; Corti et al., 2015; Johnson et al., 2016; Wang et al., 2018, 2015; Wang et al., 2016), and a polyclonal IgG has been rendered safe and tolerable in a phase 1 clinical trial (Beigel et al., 2018), there are still no MERS-CoV-specific antibody products approved for non-investigational human use.

MERS-CoV RBD-specific antibodies work by blocking receptor binding and subsequently preventing infection (Yu et al., 2015). Hypothetically, non-RBD antibodies work to sterically block receptor binding, interfere with protein rearrangement to prevent membrane fusion, or inhibit other downstream infection events, including Fc-mediated effector functions. Overall, mechanisms of action for MERS-CoV antibodies are not fully understood. In the dawn of novel MERS-CoV vaccine and antibody development, it has been increasingly important to understand MERS-CoV antibody interactions in the context of the entire S protein. To that end, developing new assays that measure antibody interactions and functionality will advance the field.

Currently, MERS-CoV antibody function is studied from two broad perspectives, binding and neutralization. Antibody binding is typically studied via methods such as ELISA, biolayer interferometry, and fluorescence-activated cell sorting (FACS). Neutralization is often assessed via pseudovirus reporter or plaque reduction neutralization (PRNT) assays in immortalized cells (Perera et al., 2013; Zhao et al., 2013). ELISA assays are limited by their inability to reliably assess antibody binding to protein antigens in their native conformation (Zhang et al., 2017). Therefore, ELISA data can sometimes be misleading and potentially generate false-positive results. For example, full-length MERS-CoV S is known to have variable RBD conformations (Pallesen et al., 2017; Yuan et al., 2017), which may differentially bind to certain antibodies. With unlimited access to those epitopes in ELISA, binding to conformationally-dependent RBD-specific antibodies may be exaggerated. An alternative to ELISA is biolayer interferometry, which utilizes a tagged antigen bound to an affinity tip. Although this method may promote uniform protein orientation, it is limited by the requirement of tagged proteins to be immobilized to the affinity tip. In addition, a previous publication has also shown biolayer interferometry may have reduced sensitivity and reproducibility (Yang et al., 2016). A major MERS-CoV antibody function is inhibition of DPP4 binding, which has to date been best studied by FACS (Pallesen et al., 2017; Wang et al., 2015). FACS methods utilize an authentically folded protein on the cell surface; however, cytometers are relatively expensive and sophisticated instruments that require management by highly-trained specialists and on-going maintenance by service engineers. FACS also requires time-consuming warm-up procedures, laser calibration, and cleaning after each use. Therefore, identifying new methods to rapidly and effectively measure antibody binding and functional properties will facilitate the evaluation and screening of antibodies for MERS-CoV and other pathogens going forward.

High-throughput cell-based antibody binding assays have been established using the Celigo Image Cytometer (Riedl et al., 2016; Zhang et al., 2017). The ability to directly image and analyze proteins or antibodies binding to target cells allows researchers to characterize binding affinity to cell surface antigens. Plate-based image cytometry can capture and analyze bright field and fluorescent images of fluorescent antibody-labeled cells directly in microplates, thus eliminating the need to disturb the natural state of cells, by methods such as lysing or trypsinization. The image cytometry workflow does not require specialized materials or time-consuming maintenance procedures to perform imaging and analysis.

Herein, we developed a high-throughput protein binding inhibition assay using the Celigo Image Cytometer. After selecting DPP4-expressing cell types and defining seeding density, MERS-CoV protein binding conditions were optimized for concentration and fluorescence staining. We then evaluated three monoclonal antibodies that recognize MERS-CoV RBD, NTD, or S2 (D12, G2, and G4, respectively) for binding inhibition of MERS-CoV S to DPP4-expressing BHK-21 cells. Finally, we quantified the ability of the three mAbs to neutralize MERS-CoV pseudovirus infection. We describe an assay that facilitates rapid measurement of protein binding to cells in a high-throughput manner. The image cytometry method is simple, high-throughput, and efficient and has good reproducibility and dynamic range. Ultimately, this method can be used for characterization of potential therapeutic antibodies against MERS-CoV or other pathogens.

2. Materials and methods

2.1. Optimization of DPP4 receptor expression on different cells types

A549 (ATCC®, CCL-185™), BHK-21 (ATCC®, CCL-10™), VeroE6 (ATCC®, CRL-1587™), and Huh 7.5 (kindly provided by provided by Deborah R. Taylor, US Food and Drug Administration, Silver Spring, MD,) cells were maintained at 37 °C under 5% CO_2 in modified Eagle's medium supplemented with 10% (v/v) fetal bovine serum and 1% Penicillin Streptomycin (growth media). Cells were plated overnight. Various amounts,0.02 – 2 μg, of plasmid encoding full-length human DPP4 were transfected into cells using Lipofectamine 3000 reagent (Invitrogen, Carlsbad, CA), following manufacturer's instructions. Two days after transfection, cells were fixed and stained for image cytometry analysis to determine DPP4 expression levels. Cell nuclei were stained with DAPI, and DPP4 receptors were stained with DPP4 PE-conjugated mouse antibody (Sino Biological, Wayne, PA) or unconjugated DPP4 rabbit polyclonal anitbodies (Abcam, Cambridge, MA) followed by anti-rabbit antibody labeled with Alexa Flour® 488 (AL488) (Abcam). Fluorescence data was exported as multiple FCS files for flow software analysis. DPP4 expression levels were analyzed by a combination of image cytometer and FlowJo 10 software (Tree Star, San Carlos, CA).

2.2. Preparation of DPP4-expressing BHK21 cells in optimized conditions

BHK-21 cells were seeded into flat bottom black-walled Greiner 96-well plates (Greiner CELLSTAR #655090) at 5×10^3 cells/well in 100 μL of media and allowed to adhere and reach 80% confluence overnight. On the following day, cells were transfected with 0.1 μg/well of DPP4 expression plasmid, using Lipofectamine 3000 reagent.

2.3. Cell-based binding inhibition assay development and analysis

Two days following DPP4 transfection, 2 μg/well of prefusion-stabilized MERS-CoV S protein (Pallesen et al., 2017) was incubated with 4-fold serial dilutions of 200 μg/mL of G2, D12, or G4 antibodies (Wang et al., 2015) for 30 min at room temperature (RT). The mixture of MERS-CoV S and mAb was then added to the DPP4-expressing BHK-21 cells and incubated for 2 h at RT. After incubation, cells were washed with PBS, fixed with 80% cold acetone for 20 min at RT, and washed again with PBS. Subsequently, 100 μL of MERS-CoV S rabbit polyclonal antibodies (Sino Biological, Beijing, China) was pipetted into each well, incubated for 60 min at RT, and washed twice. Next, secondary AL488-conjugated goat anti-rabbit IgG H&L and DPP4 PE-conjugated mouse antibody (Sino Biological) were added, incubated for 60 min at RT, and washed twice. Finally, cells were stained with 100 μL of 300 nM DAPI for 5 min and then washed 4 times prior to image cytometric analysis. Native BHK-21 cells with no cell surface DPP4 served as the negative control. In each experiment, DAPI and DPP4 PE staining served as internal controls for cell growth and DPP4 expression, respectively. Image cytometry data was exported as multiple FCS files for FlowJo analysis and as well level data for Graphpad Prism analysis. Fluorescence intensity data was gated in FlowJo to determine percent inhibition.

Percent inhibition in respect to mAb concentrations were then plotted and analyzed using Graphpad Prism with one-site-fit LogIC_{50} non-linear regression analysis. No inhibition (0%) was defined as MERS-CoV S binding to BHK21 without the addition of mAb. Full inhibition (100%) was defined as MERS-CoV S binding to BHK21 without DPP4 receptor. Sigmoidal dose response curves of Log mAb concentration versus percent inhibition were generated, and IC_{50} values were calculated.

2.4. Pseudovirus neutralization assay

Pseudovirus neutralization was assessed in BHK21 cells plated overnight in 96-well white plates and transfected with DPP4 for 2 days. Serial dilutions of mAb (starting at 66 nM, four-fold, eight dilutions) in serum-free DMEM was mixed with MERS-CoV England1 pseudovirus, which was made and titered to target 50,000 relative luciferase units (RLU), per previously-described methods (Pallesen et al., 2017; Wang et al., 2015). After incubation for 30 min at RT, media was aspirated from the previously-plated cells, and the mAb/pseudovirus mixture was added. Virus was allowed to transduce cells for 2 h at 37 °C; then fresh growth media was added. Cells were lysed at 72 h, and firefly luciferase substrate (Promega, Madison, WI) was added, per manufacturer's protocol. Relative luciferase units (RLU) were measured at 570 nm on a SpectramaxL luminometer (Molecular Devices, San Jose, CA). Sigmoidal curves were plotted from RLU averages of duplicates. Fifty percent neutralization (IC_{50}) titers were calculated considering uninfected cells as 100% neutralization and cells transduced with only pseudovirus as 0% neutralization.

2.5. Celigo Image Cytometer instrumentation, data acquisition, and analysis

Celigo Image Cytometer has been demonstrated in many high-throughput cell-based assays (Chan et al., 2016; Zhang et al., 2017). The image cytometry instrument utilizes a transmission and epi-fluorescence setup for one bright-field (BF) and four fluorescence (FL) imaging channels (Blue, Green, Red, and Far Red) with high power LED to perform plate-based image cytometric analysis. Each FL imaging channel uses a specific fluorescence filter set for the corresponding colors: Blue (EX: 377/50 nm, EM: 470/22 nm), Green (EX: 483/32 nm, EM: 536/40 nm), Red (EX: 531/40 nm, EM: 629/53 nm), and Far Red (EX: 628/40 nm, EM: 688/31 nm). The image cytometer can perform auto-focusing in the well based on the contrast of the images or the thickness of the bottom surfaces.

The Celigo software used the applications "Target 1 + 2 + Mask" and "Target 1 + 2 + 3 + Mask" to identify the DAPI-stained target cells (Blue Channel) and measuring fluorescence intensities from DPP4 PE-conjugated mouse antibody (Red Channel) and AF488-labeled goat anti-rabbit IgG H&L (Green Channel). The measured fluorescence intensity results were exported to FlowJo for further analysis of DPP4 expression and MERS-CoV S binding inhibition.

After cells were stained, the microplates were loaded and analyzed on the Celigo using preset SCAN and ANALYZE settings. For the DPP4 expression analysis, Celigo was setup to acquire images in the Target 1 (Bright Field), Target 2 (Red – PE), and Mask (Blue – DAPI), where the exposure times were 1440, 500000, and 400,000 μs, respectively. For the MERS-CoV S binding inhibition analysis, Celigo was setup to acquire images in the Target 1 (Bright Field), Target 2 (Green – Alexa Fluor® 488), Target 3 (Red – PE), and Mask (Blue – DAPI), where the exposure times were 1459, 450000, 400,000 and 400,000 μs, respectively. Next, hardware-based autofocus (HWAF) was selected to focus the cells in the Bright Field channel, where focus offsets were applied for the Green (7 μm), Blue (−6 μm), and Red (0) channels. Subsequently, the target wells were selected for image acquisition.

Image acquisition and image analysis were performed simultaneously. The preset ANALYZE parameters were used to identify DAPI-stained target cells as Mask. Next, Mask was applied to the AF488 green and PE red fluorescence channels to analyze the fluorescence intensities for each well. The fluorescence intensity results were directly exported to multiple FCS files for FlowJo analysis, and then IC_{50} values for binding inhibition were determined using GraphPad Prism. It is important to note that the fluorescence readout from the Celigo was based on the mean fluorescence intensity (MFI), which correspond to the image pixel intensity range from 0 to 255, which was translated to the fluorescent histogram scales in FlowJo.

3. Results

3.1. Selecting a high DPP4-expressing cell type for protein binding and inhibition assay

MERS-CoV utilizes DPP4 as an entry receptor into host cells. MERS-CoV S protein was used to investigate the inhibition of MERS-CoV S binding to host cells by various antibodies (G2, D12, and G4). To maximize the signal for MERS-CoV S binding, DPP4 receptors were expressed on target cells at high concentrations. For each tested cell type (A549, BHK-21, and VeroE6), transfection assays were performed with different concentrations of DNA, ranging from 0.02 to 2 μg. The concentration that produced the highest DPP4 expression was then selected: 0.1, 0.1 and 0.05 μg, for A549, BHK21 and VeroE6, respectively. Fig. 1A shows a visual comparison of DPP4 expression in A549, BHK-21, and VeroE6 cells. The left panel displays untransfected cells, while the right panel illustrates the highest DPP4 transfection for each cell type. Fluorescence intensity analysis using FlowJo is shown in Fig. 1B. DPP4 expressed least efficiently in VeroE6 cells, with only ~20% being positive for DPP4. Following transfection, A549 cells were more than 40% DPP4-positive, and BHK-21 cells were approximately 85% DPP4-positive. BHK-21 cells were thus chosen for further experiments. In addition, BHK-21 cells are known to not have endogenous DPP4 receptor. Therefore, BHK-21 cells without DPP4 transfection served as negative controls for all experiments.

3.2. Optimization of cell number for protein binding and inhibition assays

It was important to optimize cell seeding density to maximize fluorescence signals, but without overcrowding to avoid signal quenching. For that purpose, different densities of BHK-21 cells, 1×10^3–2×10^4 cells/well, were seeded overnight and transfected with DPP4. This density range was selected because most transfection protocols for 96-well plates suggest using 1–2×10^4 cells/well. In addition, based on our previous experiments, seeding 1×10^3 cells/well or lower results in a dim signal. Two days post-transfection, cell confluency and morphology were visualized and analyzed using bright field analysis (Fig. 2). Visually, 2×10^4 cells/well rendered overcrowdedness (Fig. 2A), while 1×10^3 cells/well appeared too sparse (Fig. 2C). 5×10^3 cells/well presented the optimal seeding density with no overlapping cells and even distribution throughout the well (Fig. 2B).

3.3. Development of image-based protein binding assay

The next step in assay development was to determine optimal conditions for binding of target proteins to DPP4-expressing BHK-21 cells. To optimize conditions, several parameters were tested: protein constructs (MERS-CoV S trimer or S1 monomer), protein amounts (0.1–10 μg), and staining protocol (AL488 anti-His-Tag Ab, different MERS-CoV monoclonal Abs, and AF488 anti-MERS-CoV spike Ab). It was determined that 2 μg of MERS-CoV S soluble trimer and AF488 anti-MERS-CoV spike Ab produced the best binding results (data not shown). To measure protein binding to DPP4-expressing BHK-21 cells, MERS-CoV S trimer and S1 monomer were tested; both proteins bound efficiently to the cells (Fig. 3A, B). However, FlowJo analysis of the image-based fluorescence intensity data indicated that the MERS-CoV S trimer (Fig. 3D) showed a larger peak shift (17 MFI right shifts) when

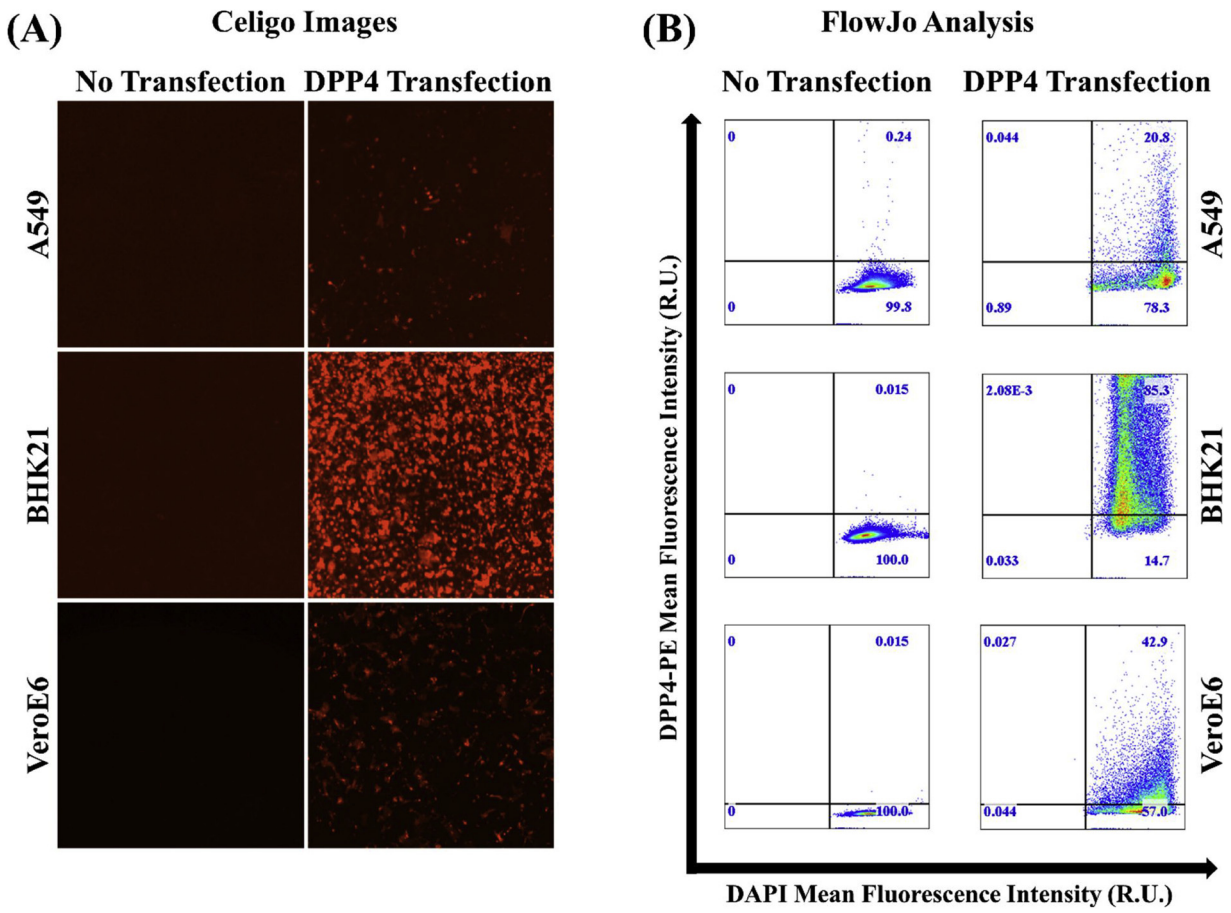

Fig. 1. Exogenously expressed DPP4 in various cell lines. Fluorescence images (A) and fluorescence intensity FlowJo analysis histograms (B) comparing untransfected A549, BHK-21, or Vero E6 cells (left panels) to cells expressing optimal amounts of DPP4, depicted by red staining (right panels).

compared to the S1 monomer (11 MFI right shifts) (Fig. 3C). In addition, utilizing MERS-CoV full-length S trimer allows the evaluation of antibody interactions with the entire S protein. Therefore, MERS-CoV S trimer was selected for subsequent inhibition experiments.

3.4. Development of image-based protein binding inhibition assay

Anti-RBD antibodies dominate host immune response to vaccination with MERS-CoV S immunogens; by blocking S from binding to DPP4, RBD-specific antibodies neutralize viral entry into host cells (Wang et al., 2015). Antibodies can also be raised to other epitopes, including NTD and S2 regions. We used mAbs that bind to different regions of MERS-CoV S to measure their ability to inhibit MERS-CoV S binding to DPP4-expressing cells. Both D12 (RBD-specific) (Fig. 4A,B) and G2 (NTD-specific, data not shown) inhibited MERS-CoV S binding in a dose-dependent manner. This phenomenon is exemplified by the fluorescence intensity of MERS-CoV S decreasing with increasing D12 mAb concentration (Fig. 4A and B). D12 binds to the same region of MERS-CoV S as DPP4 (Wang et al., 2015). The decrease in fluorescence intensity is attributable to the binding of MERS-CoV S to D12 mAb, which then prevents MERS-CoV S from binding to DPP4 expressed on BHK-21 cells. G2 binds the NTD region of MERS-CoV S which is adjacent to the RBD of its neighboring protomer. Although the G2 binding footprint does not overlap with that of DPP4 (Wang et al., 2015), these data suggest that G2 inhibits binding of MERS-CoV S to DPP4 by an unknown mechanism. It is plausible that G2 can sterically interfere with the RBD-DPP4 interaction or influence MERS-CoV S structure and stability. Binding inhibition curves reveal D12 (Fig. 4C) and G2 (Fig. 4D)

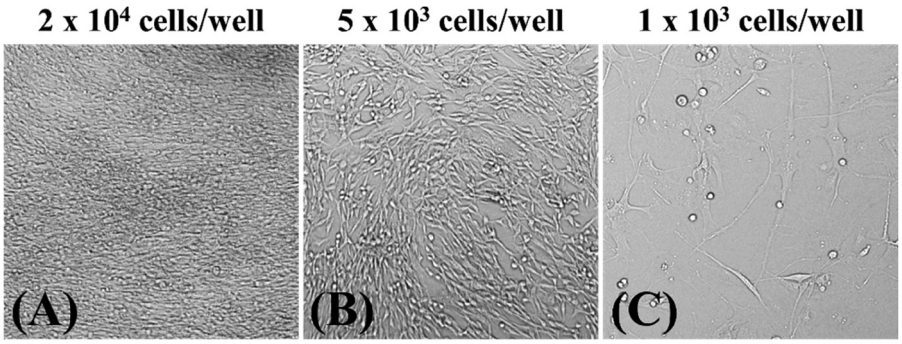

Fig. 2. Optimization of cell density for binding and inhibition assay. Bright field images of BHK-21 cells plated at various densities: 2×10^4 cells/well (A), 5×10^3 cells/well (B), 1×10^3 cells/well (C), in a 96-well plate.

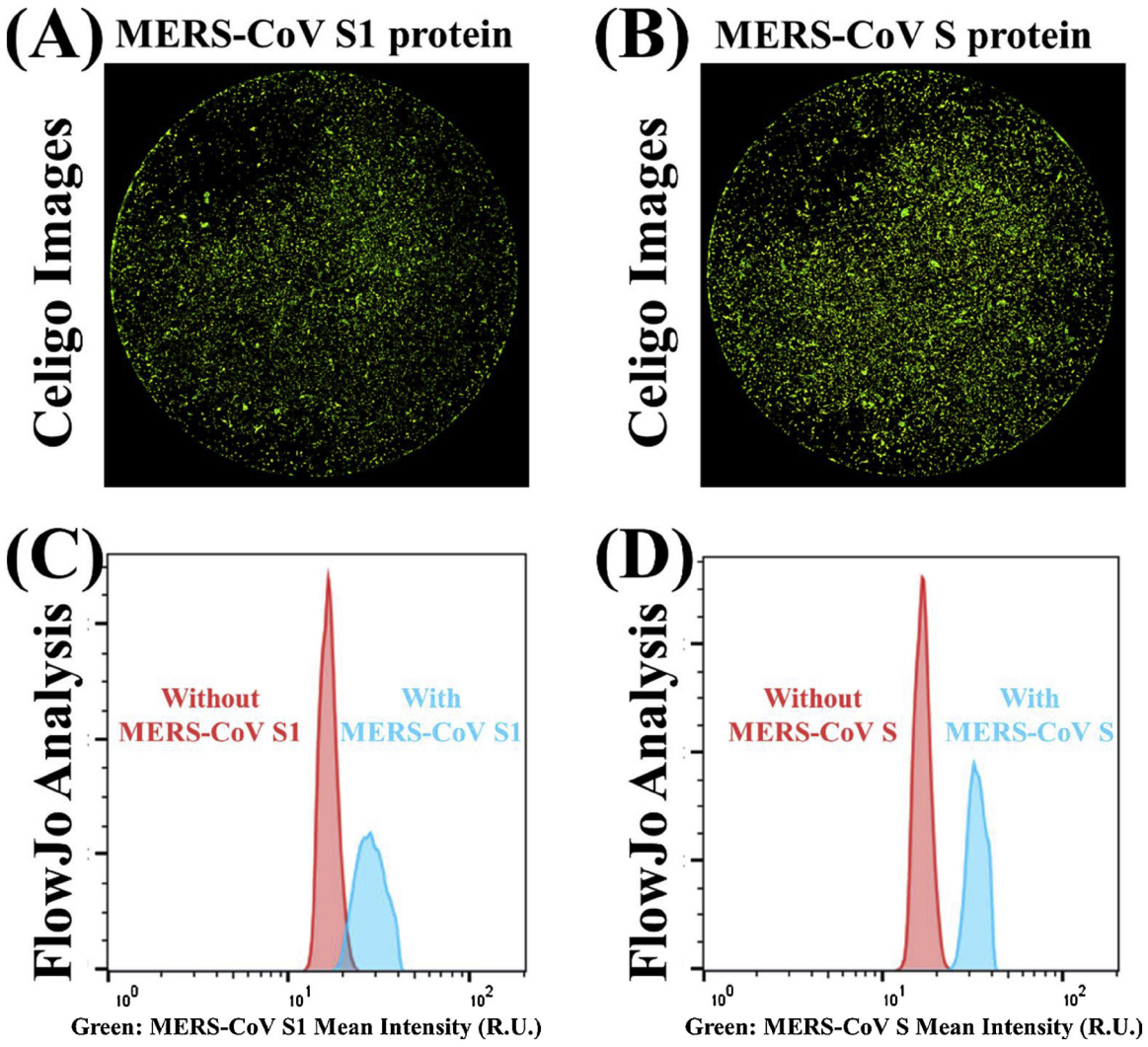

Fig. 3. MERS-CoV S1 and S proteins binding to DPP4-expressing cells. Whole well fluorescence images of MERS-CoV S1 (A) and MERS-CoV S (B) proteins binding DPP4-expressing BHK-21 cells. Both S1 monomer and S trimer proteins were stained with anti-MERS-CoV S polyclonal AL488, demonstrating binding to DPP4-expressing cells in green. FlowJo analysis of the image-based fluorescence intensity data for MERS-CoV S1 monomer (C) and S trimer (D) showed peak shifts resulting from binding.

mAbs have the same IC_{50} value (~7.5 nM), suggesting a comparable binding constant to MERS-CoV S. The results correlated to previous biolayer interferometry experiments, showing those mAbs bound to MERS-CoV S1 (Wang et al., 2015). To confirm the binding interactions being measured by image cytometer were specific to MERS-CoV S binding to DPP4, G4 was utilized. G4 binds to the S2 region, which is spatially distant from the RBD-DPP4 interaction and thus did not exhibit any inhibition effects, as expected (Fig. 4E).

3.5. Confirming binding inhibition results with antibody neutralization assay

The three mAbs tested (G2, D12 and G4) have been previously shown to effectively neutralize MERS-CoV pseudovirus in Huh 7.5 cells, which natively express DPP4 (Wang et al., 2015). Results of the inhibition assay showed that D12 and G2 mAbs inhibited MERS-CoV S binding to DPP4-expressing BHK-21 cells with similar IC_{50} values, while G4 mAb did not. Since D12 and G2 bind to the S1 region and presumably neutralize by preventing S attachment to DPP4, neutralization experiments were performed to determine whether their neutralization patterns were also similar in DPP4-expressing BHK21 cells. As expected, G2 and D12 had comparable neutralization curves (Fig. 5), with IC_{50} values in the 0.5–0.8 nM range. The reciprocal IC_{50} neutralization potency of G4 (Fig. 5) was determined to be one order of magnitude higher than D12 and G2, recapitulating binding inhibition results. The same order of magnitude difference between D12/G2 and G4 was previously shown with Huh 7.5 cells (Wang et al., 2015).

4. Discussion

Measurement of antibody specificity, magnitude, and function is critical for the development of MERS-CoV therapies and vaccines. Current assays for measuring Ab binding and neutralization have limitations and development of alternative high-throughput assays based on binding to native protein conformations in the context of the cell would be useful.

Our results demonstrated that an image cytometry-based protein binding inhibition assay can be used as a surrogate for IC_{50} determination and antibody characterization. The design of this assay resulted in a robust method to measure protein binding to antibodies or other protein ligands or assess binding competition. The variability of the newly-developed assay was assessed by including duplicates or triplicates within the same experiment and repeating identical parameters in different experiments. The coefficient of variance within the same

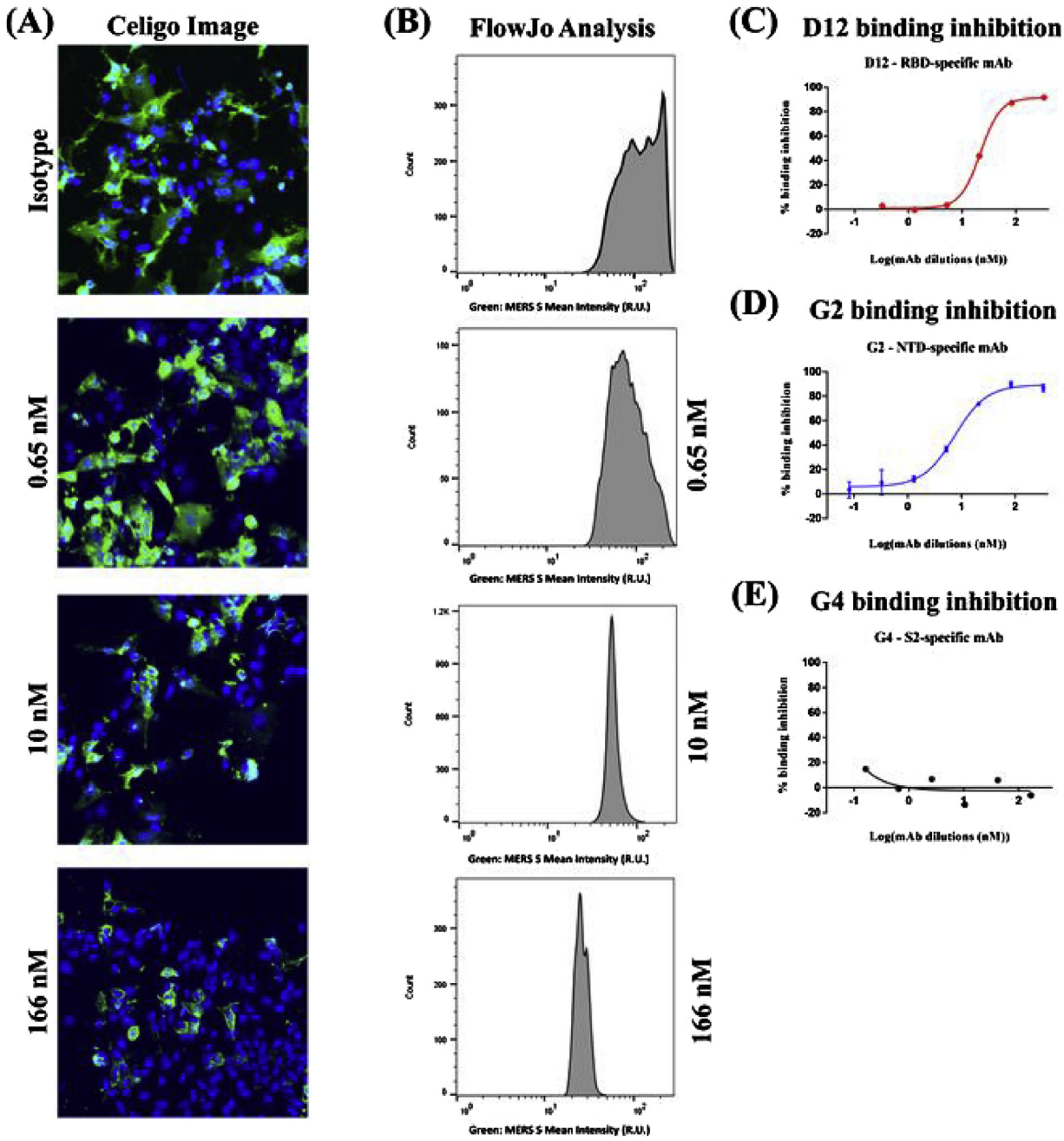

Fig. 4. Ability of mAbs to inhibit MERS-CoV S protein binding to DPP4-expressing cells. Inhibition of MERS-CoV S binding to DPP4 by D12 mAb was measured by image cytometry (A) and fluorescence intensity was analyzed by FlowJo histograms (B). As a negative control, a non-relevant isotype mAb was used. Dose response curves of Log mAb concentration versus percent inhibition were generated for D12 (C), G2 (D), and G4 (E) mAbs. (C–E) Each dot represents duplicates. Error bars represent SEM.

experiments was lower than 5% and between experiments was less than 10% (Table S1). Our binding inhibition assay combines the high-throughput benefit of ELISA with the protein conformation advantage of flow cytometry.

In this study, the efficacy of transfection was examined as a starting point for assay optimization. Transfection efficiency was measured by the mean red fluorescence intensity associated with DPP4-PE-expression in several cell types. Of note, our image cytometry method (image cytometer combined with direct conjugated DPP4 antibody) is not sensitive enough to detect low levels of endogenous DPP4 (Fig. S1). While qualitative analysis of fluorescence-based transfection is rapid, quantification requires image analysis software if performed manually. Flow cytometry systems have been adapted to automate data acquisition and analysis. Image cytometers are designed to acquire and analyze fluorescent images in a high-throughput manner. Transfection was seen in captured images, and the level of transfection could be analyzed by both internal image cytometry software and external FACS analysis software, such as FlowJo, yielding similar results. Minimal background fluorescence signals were observed in negative control groups. Also, initial experiments (optimization of DPP4 expression on different cells types) were completed in parallel by flow cytometry, and acquisition of similar results (data not shown) suggests the image cytometry method provides comparable data to FACS in a simpler format and requires less equipment maintenance than a flow cytometer.

Image cytometry has the ability to analyze the content of an entire well, which facilitates rapid optimization for assay development. Assay

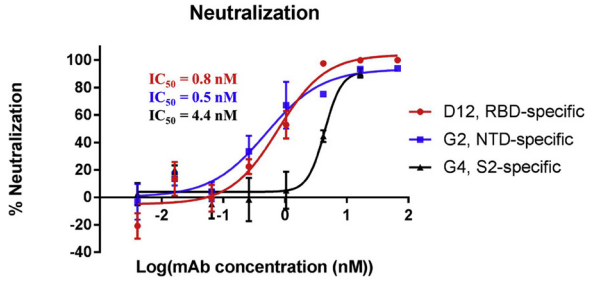

Fig. 5. Ability of mAbs to neutralize MERS-CoV in cells exogenously-expressing DPP4. Neutralization of MERS-CoV pseudovirus by D12 (red), G2 (blue), and G4 (black) in DPP4-expressing BHK-21 cells. 50% neutralization titers (IC_{50}) were calculated based on sigmoidal curves. Each dot represents duplicates. Error bars represents SEM.

parameters can be optimized more rapidly compared to flow cytometry, such as seeding density, cell type, protein selection, and staining methods. Consequently, the proposed image cytometry method can reduce experimental costs by allowing multiple replicates and various comparisons on a single plate. Scanning of all samples in a 96-well plate requires about 10–15 min and can generate results for cell count, cell morphology, and fluorescence expression (total counts, including non-transfected cells, area, mean, and integrated fluorescence intensity).

Our results demonstrated that image cytometry enabled rapid assay development resulting in a high-throughput assay to measure MERS-CoV-specific antibody function. The proposed image cytometry method can be applied to study other pathogen-antibody interactions and thus is a valuable tool for infectious diseases research in general.

Funding

This work was supported intramural funding from National Institute of Allergy and Infectious Diseases to support work at the VRC (BSG).

Conflicts of interest

NW, JSM, BSG, and KSC are inventors on US patent application no. 62/412,703, entitled “Prefusion Coronavirus Spike Proteins and Their Use”. LW, WS, YZ, WPK, and BSG are inventors on US patent application no. PCT/US2016/019395, entitled “Middle East Respiratory Syndrome Coronavirus Immunogens, Antibodies and Their Use”.

Disclosure statement

The authors LLC and PG declare competing financial interests. The research instrument used in this manuscript is a product of Nexcelom Bioscience, LLC. The work was to demonstrate a rapid protein binding and inhibition assay using the Celigo Image Cytometer.

Appendix A. Supplementary data

Supplementary material related to this article can be found, in the online version, at doi:https://doi.org/10.1016/j.jviromet.2018.11.009.

References

Beigel, J.H., Voell, J., Kumar, P., Raviprakash, K., Wu, H., Jiao, J.-A., Sullivan, E., Luke, T., Davey Jr., R.T., 2018. Safety and tolerability of a novel, polyclonal human anti-MERS coronavirus antibody produced from transchromosomic cattle: a phase 1 randomised, double-blind, single-dose-escalation study. Lancet Infect. Dis. 18, 410–418.

Chan, L.L., Smith, T., Kumph, K.A., Kuksin, D., Kessel, S., Dery, O., Cribbes, S., Lai, N., Qiu, J., 2016. A high-throughput AO/PI-based cell concentration and viability detection method using the Celigo image cytometry. Cytotechnology 68, 2015–2025.

Chen, Y., Lu, S., Jia, H., Deng, Y., Zhou, J., Huang, B., Yu, Y., Lan, J., Wang, W., Lou, Y., Qin, K., Tan, W., 2017. A novel neutralizing monoclonal antibody targeting the N-terminal domain of the MERS-CoV spike protein. Emerg. Microbes Infect. 6, e37.

Corman, V.M., Muth, D., Niemeyer, D., Drosten, C., 2018. Chapter eight - hosts and sources of endemic human coronaviruses. In: Kielian, M., Mettenleiter, T.C., Roossinck, M.J. (Eds.), Advances in Virus Research. Academic Press, pp. 163–188.

Corti, D., Zhao, J., Pedotti, M., Simonelli, L., Agnihothram, S., Fett, C., Fernandez-Rodriguez, B., Foglierini, M., Agatic, G., Vanzetta, F., Gopal, R., Langrish, C.J., Barrett, N.A., Sallusto, F., Baric, R.S., Varani, L., Zambon, M., Perlman, S., Lanzavecchia, A., 2015. Prophylactic and postexposure efficacy of a potent human monoclonal antibody against MERS coronavirus. Proc. Natl. Acad. Sci. 112, 10473–10478.

Du, L., Zhao, G., Kou, Z., Ma, C., Sun, S., Poon, V.K.M., Lu, L., Wang, L., Debnath, A.K., Zheng, B.-J., Zhou, Y., Jiang, S., 2013. Identification of a receptor-binding domain in the S protein of the novel human coronavirus middle east respiratory syndrome coronavirus as an essential target for vaccine development. J. Virol. 87, 9939–9942.

Johnson, R.F., Bagci, U., Keith, L., Tang, X., Mollura, D.J., Zeitlin, L., Qin, J., Huzella, L., Bartos, C.J., Bohorova, N., Bohorov, O., Goodman, C., Kim, D.H., Paulty, M.H., Velasco, J., Whaley, K.J., Johnson, J.C., Pettitt, J., Ork, B.L., Solomon, J., Oberlander, N., Zhu, Q., Sun, J., Holbrook, M.R., Olinger, G.G., Baric, R.S., Hensley, L.E., Jahrling, P.B., Marasco, W.A., 2016. 3B11-N, a monoclonal antibody against MERS-CoV, reduces lung pathology in rhesus monkeys following intratracheal inoculation of MERS-CoV Jordan-n3/2012. Virology 490, 49–58.

Niu, P., Zhang, S., Zhou, P., Huang, B., Deng, Y., Qin, K., Wang, P., Wang, W., Wang, X., Zhou, J., Zhang, L., Tan, W., 2018. Ultra-potent human neutralizing antibody repertoires against MERS-CoV from a recovered patient. J. Infect. Dis.

Pallesen, J., Wang, N., Corbett, K.S., Wrapp, D., Kirchdoerfer, R.N., Turner, H.L., Cottrell, C.A., Becker, M.M., Wang, L., Shi, W., Kong, W.-P., Andres, E.L., Kettenbach, A.N., Denison, M.R., Chappell, J.D., Graham, B.S., Ward, A.B., McLellan, J.S., 2017. Immunogenicity and structures of a rationally designed prefusion MERS-CoV spike antigen. Proc. Natl. Acad. Sci. 114, E7348–E7357.

Perera, R.A., Wang, P., Gomaa, M.R., El-Shesheny, R., Kandeil, A., Bagato, O., Siu, L.Y., Shehata, M.M., Kayed, A.S., Moatasim, Y., Li, M., Poon, L.L., Guan, Y., Webby, R.J., Ali, M.A., Peiris, J.S., Kayali, G., 2013. Seroepidemiology for MERS coronavirus using microneutralisation and pseudoparticle virus neutralisation assays reveal a high prevalence of antibody in dromedary camels in Egypt, June 2013. Eurosurveillance 18, 20574.

Raj, V.S., Mou, H., Smits, S.L., Dekkers, D.H.W., Müller, M.A., Dijkman, R., Muth, D., Demmers, J.A.A., Zaki, A., Fouchier, R.A.M., Thiel, V., Drosten, C., Rottier, P.J.M., Osterhaus, A.D.M.E., Bosch, B.J., Haagmans, B.L., 2013. Dipeptidyl peptidase 4 is a functional receptor for the emerging human coronavirus-EMC. Nature 495, 251.

Riedl, T., van Boxtel, E., Bosch, M., Parren, P.W., Gerritsen, A.F., 2016. High-throughput screening for internalizing antibodies by homogeneous fluorescence imaging of a pH-activated probe. J. Biomol. Screen. 21, 12–23.

Wang, L., Shi, W., Chappell, J.D., Joyce, M.G., Zhang, Y., Kanekiyo, M., Becker, M.M., van Doremalen, N., Fischer, R., Wang, N., Corbett, K.S., Choe, M., Mason, R.D., Van Galen, J.G., Zhou, T., Saunders, K.O., Tatti, K.M., Haynes, L.M., Kwong, P.D., Modjarrad, K., Kong, W.-P., McLellan, J.S., Denison, M.R., Munster, V.J., Mascola, J.R., Graham, B.S., 2018. Importance of neutralizing monoclonal antibodies targeting multiple antigenic sites on MERS-CoV Spike to avoid neutralization escape. J. Virol. 92 (May (10)), e02002–e02017.

Wang, L., Shi, W., Joyce, M.G., Modjarrad, K., Zhang, Y., Leung, K., Lees, C.R., Zhou, T., Yassine, H.M., Kanekiyo, M., Yang, Z.-y., Chen, X., Becker, M.M., Freeman, M., Vogel, L., Johnson, J.C., Olinger, G., Todd, J.P., Bagci, U., Solomon, J., Mollura, D.J., Hensley, L., Jahrling, P., Denison, M.R., Rao, S.S., Subbarao, K., Kwong, P.D., Mascola, J.R., Kong, W.-P., Graham, B.S., 2015. Evaluation of candidate vaccine approaches for MERS-CoV. Nat. Commun. 6, 7712.

Wang, N., Shi, X., Jiang, L., Zhang, S., Wang, D., Tong, P., Guo, D., Fu, L., Cui, Y., Liu, X., Arledge, K.C., Chen, Y.-H., Zhang, L., Wang, X., 2013. Structure of MERS-CoV spike receptor-binding domain complexed with human receptor DPP4. Cell Res. 23, 986.

Wang, W., Wang, H., Deng, Y., Song, T., Lan, J., Wu, G., Ke, C., Tan, W., 2016. Characterization of anti-MERS-CoV antibodies against various recombinant structural antigens of MERS-CoV in an imported case in China. Emerg. Microbes Infect. 5, e113.

WHO, 2018. Middle East Respiratory Syndrome Coronavirus (MERS-CoV). World Health Organization.

Yang, D., Singh, A., Wu, H., Kroe-Barrett, R., 2016. Comparison of biosensor platforms in the evaluation of high affinity antibody-antigen binding kinetics. Anal. Biochem. 508, 78–96.

Yu, X., Zhang, S., Jiang, L., Cui, Y., Li, D., Wang, D., Wang, N., Fu, L., Shi, X., Li, Z., Zhang, L., Wang, X., 2015. Structural basis for the neutralization of MERS-CoV by a human monoclonal antibody MERS-27. Sci. Rep. 5, 13133.

Yuan, Y., Cao, D., Zhang, Y., Ma, J., Qi, J., Wang, Q., Lu, G., Wu, Y., Yan, J., Shi, Y., Zhang, X., Gao, G.F., 2017. Cryo-EM structures of MERS-CoV and SARS-CoV spike glycoproteins reveal the dynamic receptor binding domains. Nat. Commun. 8, 15092.

Zhang, H., Chan, L.L., Rice, W., Kassam, N., Longhi, M.S., Zhao, H., Robson, S.C., Gao, W., Wu, Y., 2017. Novel high-throughput cell-based hybridoma screening methodology using the Celigo Image Cytometer. J. Immunol. Methods 447, 23–30.

Zhao, G., Du, L., Ma, C., Li, Y., Li, L., Poon, V.K.M., Wang, L., Yu, F., Zheng, B.-J., Jiang, S., Zhou, Y., 2013. A safe and convenient pseudovirus-based inhibition assay to detect neutralizing antibodies and screen for viral entry inhibitors against the novel human coronavirus MERS-CoV. Virol. J. 10, 26.